

Article

Extreme Learning Machine-Based Diagnostics for Component Degradation in a Microturbine

Nicola Menga¹ , Akhila Mothakani¹, Maria Grazia De Giorgi¹ , Radoslaw Przysowa^{2*}  and Antonio Ficarella¹ 

¹ Department of Engineering for Innovation, University of Salento, 73100 Lecce, Italy; nicola.menga@unisalento.it (N.M.); akhila.mothakani@studenti.unisalento.it (A.M.); mariagrazia.degiorgi@unisalento.it (M.G.D.G.); antonio.ficarella@unisalento.it (A.F.)

² Instytut Techniczny Wojsk Lotniczych (ITWL), ul. Księcia Bolesława 6, 01-494 Warsaw, Poland

* Correspondence: radoslaw.przysowa@itwl.pl

Abstract: Micro turbojets are used for propelling radio-controlled aircraft, aerial targets and personal air vehicles. When compared to full-scale engines, they are characterized by relatively low efficiency and durability. In this context, the degraded performance of gas path components could lead to an unacceptable reduction in the overall engine performance. In this work, a data-driven model based on a conventional Artificial Neural Network (ANN) and an extreme learning machine (ELM) was used for estimating the performance degradation of the micro turbojet. The training datasets containing the performance data of the engine with degraded components were generated using the validated GSP model and the Monte Carlo approach. In particular, compressor and turbine performance degradation were simulated for three different flight regimes. It was confirmed that component degradation has a higher impact in flight than at sea level. Finally, the datasets were used in the training and testing process of the ELM algorithm with four different input vectors. Two vectors had an extensive number of virtual sensors, and the other two were reduced to just fuel flow and Exhaust Gas Temperature. Even with the small number of sensors, the high prediction accuracy of ELM was maintained for takeoff and cruise but was slightly worse for variable flight conditions.

Keywords: ELM; ANN; compressor; turbine; degradation; microturbine; engine health management



Citation: Menga, N.; Mothakani, A.; De Giorgi, M.G.; Przysowa, R.; Ficarella, A. Extreme Learning Machine-Based Diagnostics for Component Degradation in a Microturbine. *Preprints* **2022**, *1*, 0. <https://doi.org/>

Publisher's Note: MDPI stays neutral with regard to jurisdictional claims in published maps and institutional affiliations.



Copyright: © 2022 by the authors. Licensee MDPI, Basel, Switzerland. This article is an open access article distributed under the terms and conditions of the Creative Commons Attribution (CC BY) license (<https://creativecommons.org/licenses/by/4.0/>).

1. Introduction

In operation, engine components face several physical problems such as fouling, erosion, corrosion, blade damage, excessive tip clearance, worn seals, combustor damage, and many others. The performance of the engine will deteriorate and this performance loss depends on the type and severity of the deterioration and the components that are affected. Component degradation means a decrease in its efficiency, which leads to an increase in fuel consumption and exhaust gas temperature (EGT). Generally, a deteriorated gas turbine provides less thrust for a certain amount of fuel flow or needs more fuel to produce a certain amount of thrust. For the user, predicting Remaining Useful Life (RUL) is most important because it makes possible to plan maintenance in advance and take informed go/no do decisions. The main factors that prevent the continued operation of the engine are the loss of the surge margin of the compressor [1] and the exceeding of the maximum operating temperature of the turbine i.e. loss of the temperature margin. [2].

Modeling the dynamics of a complex non-linear system, such as a gas turbine, makes it possible to control it effectively and monitor its performance [3]. A reliable model is necessary to simulate engine operation under off-design and degraded conditions and to predict the loss in performance of engine components. There are many solutions to this problem for full scale engines [4,5]. An integrated health monitoring platform for performance analysis and degradation diagnostics of gas-turbine engines was demonstrated in our earlier project [6,7]. Ellis et al. modeled the deposition of ingested particles on turbine nozzle guide vanes to predict high-pressure turbine degradation using Monte Carlo simulations and a zero-dimensional turbofan model [8]. However, component degradation

is less studied for microturbines, which are more and more used both in distributed energy systems [9,10] and in Unmanned Aerial Vehicles (UAV) [11,12].

Microturbines, small turbojets or turboprops are manufactured in a wide range of classes [13,14]. They are often operated outside regular airports or power stations and are thus prone to ingesting environmental particles. In such conditions, their compressor and turbine may rapidly degrade, so it is essential to monitor and predict performance degradation [15,16]. Coupling sensor data with model predictions makes it possible to monitor engine parameters for fault diagnosis and manage component deterioration [17,18].

Performance parameter (PP) is any operating variable of the engine depending on the physical condition of its components, which affects the engine output (thrust or power) and fuel consumption [19]. Engine parameters under off-design and degraded conditions could be estimated or predicted by machine learning techniques. Among various approaches, Artificial Neural Networks (ANNs) are widely used for diagnostic purposes nowadays due to their ability to recognize the complex relations between different physical parameters with high accuracy. This characteristic is used in engine health monitoring systems (EHM) to predict the values of the non-measurable performance parameters used as health status of the monitored components (or overall engine) based on some other measurable parameters by means of adequate sensor installed through the powertrain, such as temperature and pressure in various engine stations, shaft speed, fuel flow, torque and others.

Different types of ANN-based techniques are used for fault detection in aircraft engine purposes [4,20,21]. Recently, many efforts were dedicated to the Extreme Learning Machine (ELM) [22,23], which turns out to be more efficient than the classical feed-forward neural network but is still less widespread. Zhao et al. confirmed better performance provided by Soft Extreme Learning Machine (SELM) and Improved SELM (ISELM) [24]. To improve numerical stability, a regularization term is often used in ELM diagnostic systems [25–27]. Liu et al. introduced the optimized ELM based on restricted Boltzmann machine [28] to predict the *EGT* trend in Auxiliary Power Unit (APU) with the improved stability of ELM solutions when some input parameters are correlated. Bai et al. applied a long-short term memory (LSTM) network for fault detection of three-shaft marine gas turbine [29]. Online sequential extreme learning machines (OS-ELM) are used for data-driven engine modeling [30–32]. These studies underlined the suitability of Artificial Intelligence tools to predict engine performance with high accuracy. However, few works deal with the implementation of such models for micro and small gas-turbine engines.

Traditional engine models rely on the thermodynamic description of the engine, so they are called white-box or physics-based approaches. Such a model of a micro turbojet [33] was recently developed and fine-tuned in GSP (Gas turbine Simulation Program) [34,35], and validated with experimental flight data. This model was reused here for generating training datasets for an artificial neural network (ANN), for a planned engine health management system.

In this work, steady-state simulations were performed using the model in the presence of different degradation severity conditions for the turbine and compressor components. The datasets were obtained using a Monte Carlo approach to generate the different operating conditions to be simulated. Then the data predicted by the aeroengine model were used as input of the ELM neural network to predict the degradation level of the compressor and turbine in several engine operating conditions, on the ground and in flight.

2. Materials and Methods

2.1. Micro Turbojet

The engine studied in this work is JetCat P140 Rxi-B (Table 1), propelling a prototype aerial target. This engine is also used in radio-controlled (RC) models and some Personal Aircraft Vehicles (PAV). It is a micro turbojet, controlled by the Electronic Control Unit (ECU), with a radial compressor, axial turbine, electrical starter and fuel pump [36]. The main shaft is supported on two high-speed ceramic ball bearings, lubricated with a blend of

fuel and oil in an open system. They have a short life, so the recommended service interval of the engine is only 25-50 flight hours.

Table 1. Jetcat P140 Rxi-B engine specifications [36]

Parameter	Specification	
Overall Pressure Ratio	3.4	
Air flow rate	0.35	kg/s
Maximum <i>EGT</i>	749	C
Mass Flow	0.34	kg/s
Maximum Thrust	142	N
Design Speed	125	kRPM
Fuel consumption	7.33	g/s

The propelled aerial target is used for training air defense. This twin-engine drone imitates enemy fighters by offering similar flight parameters, radar foot-print and thermal signature [37]. It takes off from a catapult and lands on a parachute, so its engines are less exposed to gas-path contamination than whose of RC aircraft which often operate from unmaintained runways. However, in high maneuver missions, rotor-stator contacts are possible which can lead to increased tip clearance and reduced efficiency.

The engine model was developed in GSP, which is an object-oriented 0D simulation environment where the mean flow properties are calculated only at the inlet and the output of the components while the field inside them is not parsed. GSP deployed and incorporated a set of nonlinear differential equations describing thermodynamic cycles and rotor dynamics.

The adopted structure of the engine model (Figure 1) follows the standard turbojet template. All the components were configured to accurately model the engine behavior by setting their design parameters, such as the maximum speed, pressure ratio, mass flow rate, fuel flow rate, efficiencies, and so forth. The model was used to simulate the design point, steady states at various engine speeds and transient operation, at sea level and in flight conditions [33]. The engine model was validated with data gathered from bench tests and the flight missions of the twin-engine aerial target.

The degradation was simulated in GSP by changing the corresponding health parameters of the components, given by the efficiency and the flow coefficient for the compressor and the turbine. To produce more operating points, the assumed degradation levels of components were defined in the GSP Monte Carlo input controller. GSP implements a random generator with inverse normal cumulative distribution function to calculate input parameters for the simulation based on the given mean value and standard deviation [35]. For this input data, GSP produces engine model outputs for varying degradation levels, appropriate for training ANN. It is practically impossible to obtain similar datasets from real flights.

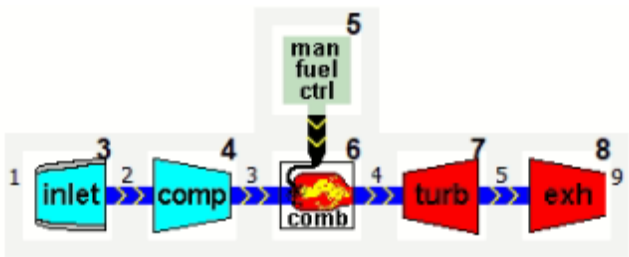


Figure 1. Turbojet model in GSP.

2.2. Prediction of Component Degradation

In this study, component deterioration is considered for the single-stage radial compressor and axial turbine. The severity of component deterioration is characterized by the difference between the actual component condition parameters and their baseline. From a thermodynamic perspective, the condition of gas path components is quantified by isentropic efficiency η and mass flow W . Even if the degradation of the microturbine causes significant variation in component flow and efficiency, these parameters cannot be directly measured and so used to identify the engine health condition. However, some parameters measured by the sensors installed inside the engine, such as temperature, pressure, rotating speed etc., will be affected by component degradation and can be used for the engine health status prediction.

Figure 2 describes the methodology adopted in this work. The degradation prediction procedure includes the following steps :

1. The rig and flight data acquired from a real micro turbojet were used to validate the GSP model [33]. The validated model was subsequently used to simulate selected operating conditions in order to obtain the values of the virtual engine sensors, necessary to train and test the predictive techniques. The simulated parameters are listed in Table 2.
2. Three simulated flight regimes: 1) Takeoff, 2) Cruise and 3) Air mission were defined by different Mach (M) and altitude (Z_p) values (Table 3). Additionally, M and Z_p were randomly distributed in flight regime 3. For each operating regime, the data generated by GSP embrace 500 operating points, 450 for training and 50 for testing.
3. Both clean and degraded conditions of the compressor and the turbine were simulated. Two degraded performance parameters (efficiency and mass flow) were analyzed for each component (compressor and turbine). The expected variability of the chosen performance parameters needs a huge amount of simulated data to completely cover this multidimensional space by the AI regression model. Hence, each of the four performance parameters was assigned random values to simulate different level of degradation severity using the GSP Monte Carlo input controller by selecting their mean value (-10%) and standard deviation (2%).
4. From the virtual sensors, four input vectors for training AI models were selected, as reported in Table 4. Input vector 1 consists of ten virtual sensors used for flight regimes 1 and 2 excluding speed and ambient conditions which are constant. Input vector 2, used for flight regime 3, has a complete set of 13 parameters. Input vector 3, used for flight regimes 1 and 2, has only two parameters that correspond to the real sensors installed on the microturbine: W_f and EGT . Input vector 4 used for flight regime 3 includes M , $TT1$, $PT1$, W_f and EGT .
5. The datasets generated by the GSP were used for training and testing ANN/ELM models to validate their accuracy in predicting the component efficiency η and mass flow W . The comparison between ANN and ELM was performed on the input vectors 1 and 2. After that, the reduced input vectors 3 and 4 were used to verify the ELM prediction accuracy for all the degraded flight regimes.

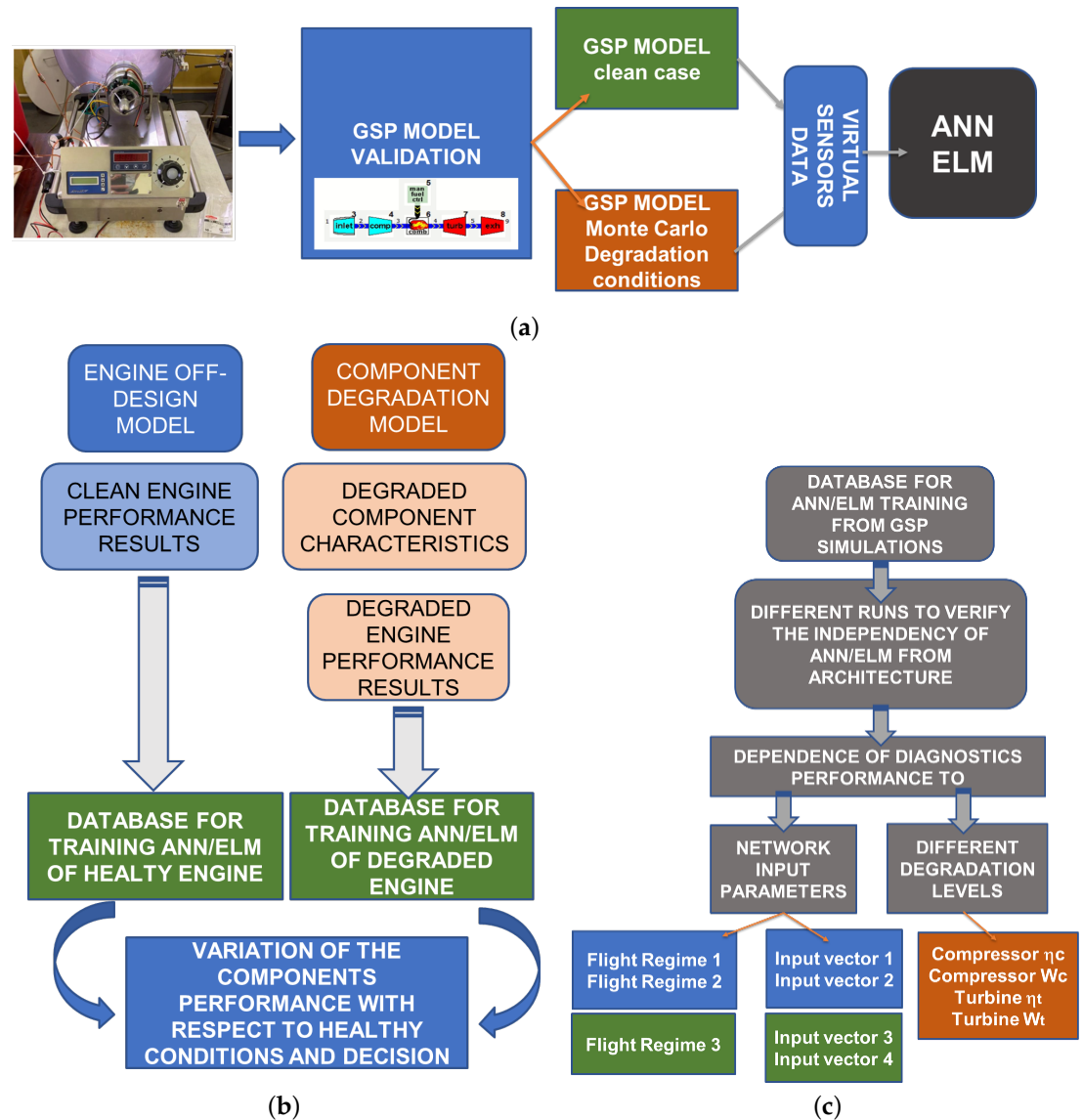


Figure 2. Methodology for component degradation prediction

Table 2. Virtual sensors: simulated engine parameters

Symbol	Parameter
TT_1	ambient total temperature
PT_1	ambient total pressure
M	Mach number
W_f	fuel flow
PT_{outC}	compressor outlet total pressure
TT_{outC}	compressor outlet temperature
PR_C	compressor pressure ratio
PR_T	turbine pressure ratio
PT_{inT}	turbine inlet total pressure
TT_{inT}	turbine inlet temperature
PT_{outT}	turbine outlet total pressure
TT_{outT}	turbine outlet temperature
PT_N	nozzle outlet total pressure
EGT	exhaust gas temperature

Table 3. Ambient conditions and nondegraded component performance in simulated flight regimes

Flight regime		Altitude	Air Speed	Compressor efficiency	Compressor mass flow	Turbine efficiency	Turbine mass flow
		Z_p [m]	M	η_c	$W_{g,c}$ [kg/s]	η_t	$W_{g,t}$ [kg/s]
1	Takeoff	0	0	0.740	0.350	0.750	0.359
2	Cruise	3000	0.3	0.737	0.271	0.739	0.275
3	Air mission	3000± 700	0.2± 0.05	0.733-0.740	0.209-0.350	0.719-0.750	0.212-0.359
Degradation (mean ± std deviation)				-10± 2 %	-10± 2 %	-10± 2 %	-10± 2 %

Table 4. Input vectors for ML models

Input Vector	Vector length	Parameters	Flight regime	ML model
1	10	$W_f, PT_{outC}, TT_{outC}, PR_C, PR_T, PT_{inT}, TT_{inT}, PT_{outT}, TT_{outT}, PT_N$	1,2	ANN/ELM
2	13	$M, TT_1, PT_1, W_f, PT_{outC}, TT_{outC}, PR_C, PR_T, PT_{inT}, TT_{inT}, PT_{outT}, TT_{outT}, PT_N$	3	ANN/ELM
3	2	W_f, EGT	1,2	ELM
4	5	M, TT_1, PT_1, W_f, EGT	3	ELM

2.3. Machine Learning Techniques

Due to their performance and versatility, machine learning methods are more and more widespread, for different purposes. In our earlier project, Nonlinear AutoRegressive with eXogenous inputs (NARX) neural networks (adequate for time-series data) were used to predict the Exhaust Gas Temperature (*EGT*) with a one-step-ahead approach [38]. Results show a percentage error which almost always remains below 10% in absolute value. The *EGT* values were obtained by adopting another artificial intelligence technique, i.e. multigene genetic programming. NARX were also used to estimate specific fuel consumption during transient regimes [39]. More in detail, the developed system was composed of two different ANNs, the first one used to predict some engine parameters based on flight data and the second to predict the specific fuel consumption based on the parameters predicted from the first ANN and flight data. Results show good performance both in healthy and degraded conditions.

We also applied separately ANN and Support Vector (SVM)-based tools to the case of a single-spool turbojet for analyzing compressor and turbine degradation [6]. The results show very good performance, in particular ANN gives better results in performance prediction, while SVM leads in engine health status prediction. Recently, we applied Feed-Forward Neural Networks (FFNNs) and Kernel Principal Component Analysis (KPCA) to estimate degraded performance of PW200 turboshaft [40].

Here, we focus on modeling JetCat turbojet performance and predicting its component degradation with AI-based regression algorithms, such as ANN and ELM. Unlike some other methods, only the current level of degradation is predicted, without taking into account past or future trends. This approach is well suited for micro turbojets, which have a short wing life and thus produce too little data to analyze their wear in a wider time prospective.

2.3.1. ANN-based regression

ANNs are machine learning-based tools which implement a virtual version of the human nervous system and of his capacity to learn from experience. A typical ANN is formed by neurons, in turn arranged in layers. Information fed in an ANN pass through an input layer, one or more hidden layers and an output layer. Each neuron in a layer is linked with the neurons of the adjacent layers by means of connections, having its own

weight. Input, hidden(s) and output layers are formed by the so-called input, hidden and output neurons respectively. The number of input and output neurons are equal to the number of features given in input and to the number of variables to be predicted respectively. The number of hidden layers and neurons are arbitrarily and directly affect the ANN performance. Figure 3, report a typical architecture of an ANN type used in this work.

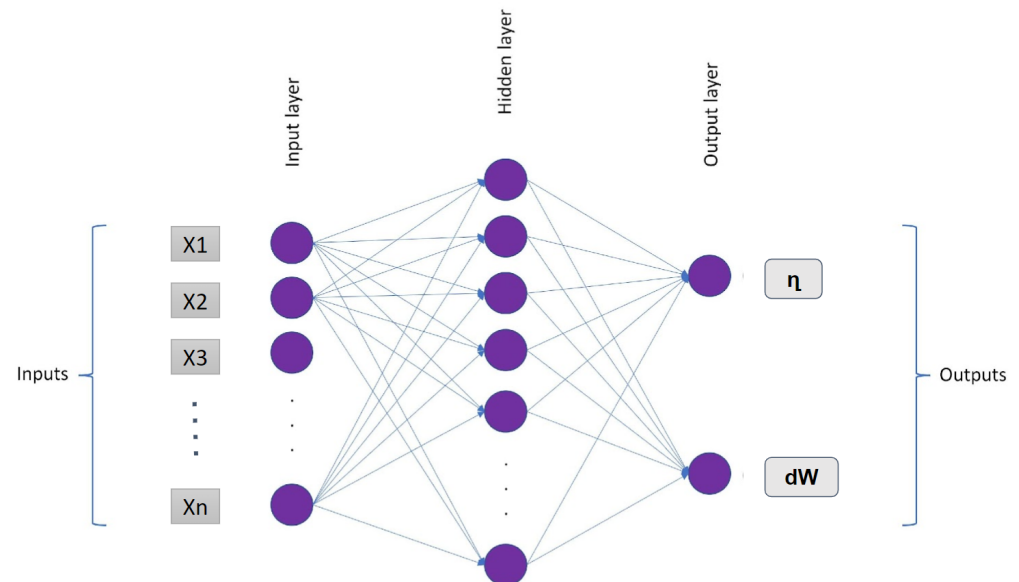


Figure 3. Structure of ANN with one hidden layer.

Each neuron located in hidden and output layers work by performing a weighted sum of the information received from the previous neurons and adding a bias. This process is described by the following equation:

$$z = \sum_{i=1}^n W_i I_i + b \quad (1)$$

where z represents the calculation result, W_i is the weight of the link between the neuron in question and the i -th neuron from which it receives information, I_i is the information received by the i -th neuron, n is the number of previous neurons that send information to the neuron in question and b is the bias. The neuron output is finally subject to an activation function, in order to normalize it. Weights and biases are computed in the training phase. During the training process, the ANN is informed with a series of example cases, including both the input features and the corresponding variables to be predicted. This serves to lead the ANN to calculate the proper weights and biases in order to obtain a small error between the predictions and the real values to be predicted.

2.3.2. ELM-based Regression

Extreme Learning Machine (ELM), introduced by Huang [22], is one of the most modern AI-based machine learning approaches. It has the single-layer feed-ahead neural network (SLFN) architecture in which the weights of hidden layers are randomly set while the output ones are analytically determined via linear algebra operations. ELM was firstly implemented for the single hidden layer feed-forward neural networks and then was extended to the generalized SLFNs wherein the hidden layer no longer has to be neuron alike.

Unlike the traditional FFNN models, the hidden layer does not need to be tuned in ELM. The output characteristic of ELM for generalized SLFNs (for one output node case as an example) is

$$f_L(x) = \sum_{i=1}^L \beta_i h_i(x) = h(x)\beta \quad (2)$$

in which $\beta = [\beta_1, \dots, \beta_L]^T$ is the vector of the output weights among the hidden layer of L nodes and the output node, and $h(x) = [h_1(x), \dots, h_L(x)]$ is the output (row) vector of the hidden layer with respect to the input x . $h(x)$ virtually maps the records from the d -dimensional center area to the L -dimensional hidden-layer characteristic area (ELM characteristic area) H , and thus, $h(x)$ is certainly a characteristic mapping.

Unlike conventional learning algorithms, ELM tends to attain no longer the smallest training error but additionally the smallest norm of output weights. According to Bartlett's theory, for feedforward neural networks to attain smaller prediction errors, the smaller the norms of weights are, the higher generalization overall performance the networks generally tend to have. We conjecture that this could be real to the generalized SLFNs in which the hidden layer will not be neuron-like. ELM is to reduce the training error in addition to the norm of the output weights.

Minimize $\|H\beta - T\|^2$ and $\|\beta\|$ where T is the target output and H is the hidden-layer output matrix:

$$H = \begin{bmatrix} h(x_1) \\ \vdots \\ h(x_N) \end{bmatrix} = \begin{bmatrix} h_1(x_1) & \dots & h_L(x_1) \\ \vdots & \vdots & \vdots \\ h_1(x_N) & \dots & h_L(x_N) \end{bmatrix} \quad (3)$$

The minimum norm least square technique as opposed to the traditional optimization technique became used in the implementation of ELM. The output weights can be obtained by the following formula:

$$\beta = H^+ T \quad (4)$$

in which H^+ is the Moore–Penrose generalized inverse of a matrix H . Different techniques may be used to calculate the Moore–Penrose generalized inverse of a matrix: orthogonal projection approach, orthogonalization approach, iterative approach, and singular value decomposition (SVD). The orthogonal projection approach may be utilized if $H^T H$ is nonsingular and $H^+ = (H^T H)^{-1} H^T$, or HH^T is nonsingular and $H^+ = H^T (HH^T)^{-1}$.

In this work, the implemented ELM model consists of three layers: the input layer (input vector 1/2/3), the hidden layers (neurons) and the output layer (η_C and dW_C , or η_T and dW_T , Figure 4).

The ELM network was implemented in three steps:

1. Randomly initialize the initial weights and thresholds of the ELM network and set the activation function.
2. Calculate the hidden layer output matrix and the generalized matrix.
3. Calculate the output matrix.

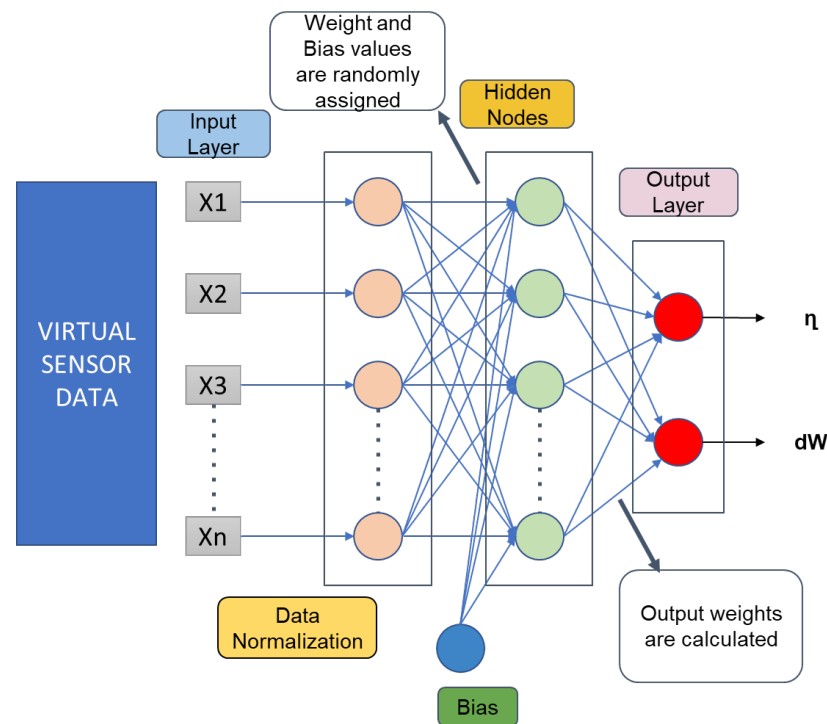


Figure 4. Structure of the ELM network.

3. Results and Discussion

3.1. Engine performance simulations

The aeroengine performance under different degradation conditions was simulated in GSP. Figures 5 and 6 show the correlation between compressor efficiency and turbine efficiency respectively with the thrust (F) and the Thrust Specific Fuel Consumption (TSFC) both at sea level (Flight regime 1) and at cruise (Flight regime 2) for different degradation levels. The trend is the same for both components. An increase in efficiency leads to a rise in F and a decrease in TSFC. The variation of the microturbine performance due to the degradation of the components is higher at $M=0.3$ than at sea level. While in healthy configuration, TSFC changes little with Mach number, the difference of TSFC between $M=0$ and $M=0.3$ significantly increases in the presence of high degradation.

Figure 7 shows the variation of Mach number and altitude operating conditions in flight regime 3, generated by the Monte-Carlo method in GSP. The operating points are independent and presented in a random order, so they do not form a trend or time series.

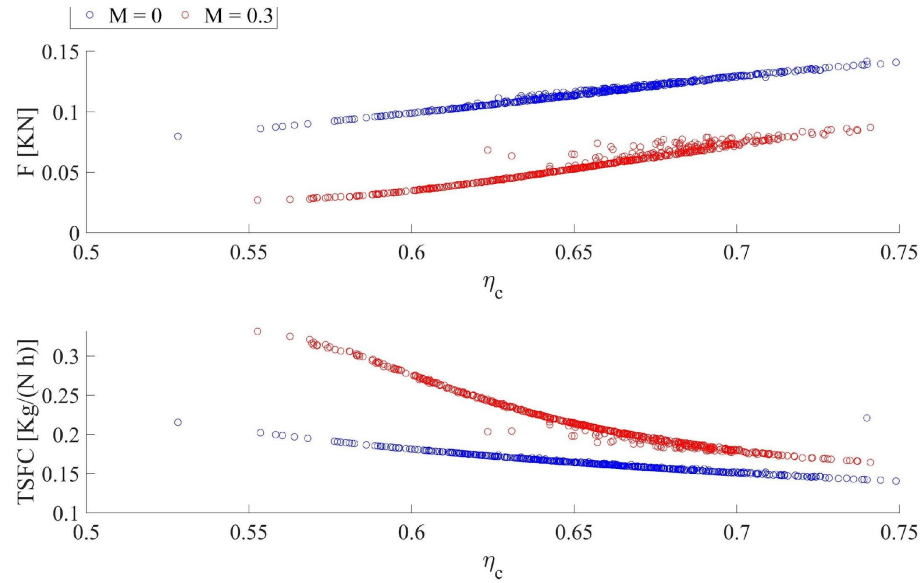


Figure 5. Thrust F and TSFC vs compressor efficiency η_c at sea level and cruise conditions for different degradation levels.

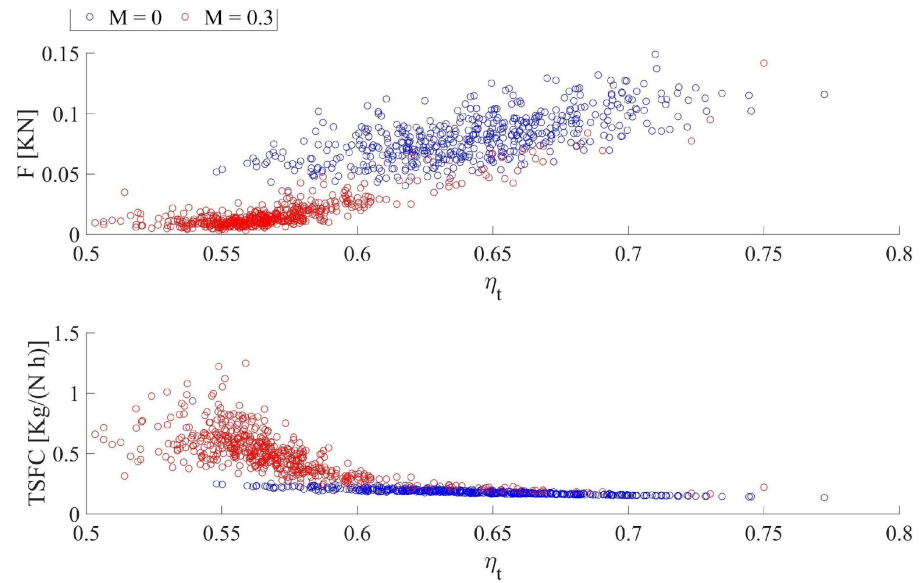


Figure 6. Thrust F and TSFC vs turbine efficiency η_t at sea level and cruise conditions for different degradation levels.

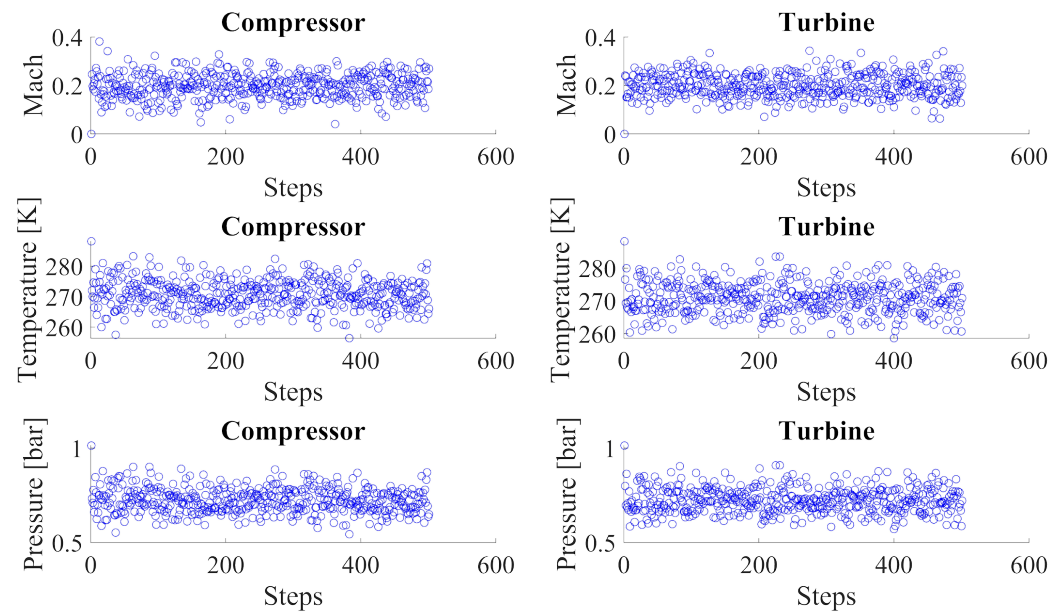


Figure 7. Airspeed, ambient temperature and pressure for the randomly generated points by the Monte-Carlo method

3.2. ANN and ELM predictions with Input vectors 1 and 2

In this sections the predicted performance parameters of the two components is compared with the target virtual sensors data. The relative error is shown to evaluate the prediction accuracy.

Firstly, the condition at sea level was investigated for both compressor and turbine degradation (Flight regime 1). Figures 8 and 9 show the results of ANN and ELM predictions in the case of compressor and turbine degradation respectively. Target and predicted results were compared for test data in addition with the percentage prediction errors.

Figure 10 and 11 show the results of ANN and ELM predictions at the flight regime 2 ($M=0.3$, $Z_p=3000$ m), that is the cruise operating condition for the compressor and the turbine. The good prediction performances are still evident for both methods. In particular for η_c prediction, ELM shows visible better performance compared with the ANN, which otherwise shows acceptable results, with only a peak in percentage error which approach 1.2%. In the prediction of $W_{g,c}$ instead, both ANN and ELM show very low percentage errors. Results are good also for the prediction of the parameters related to the turbine, except for a single point, in which the value to be predicted (both for η_t and $W_{g,t}$) differs from the target in the case of ANN. This error peak corresponds to a value of the η_t of 0.75 that is a condition in the queues of the normal distribution of η_t generated by Montecarlo method.

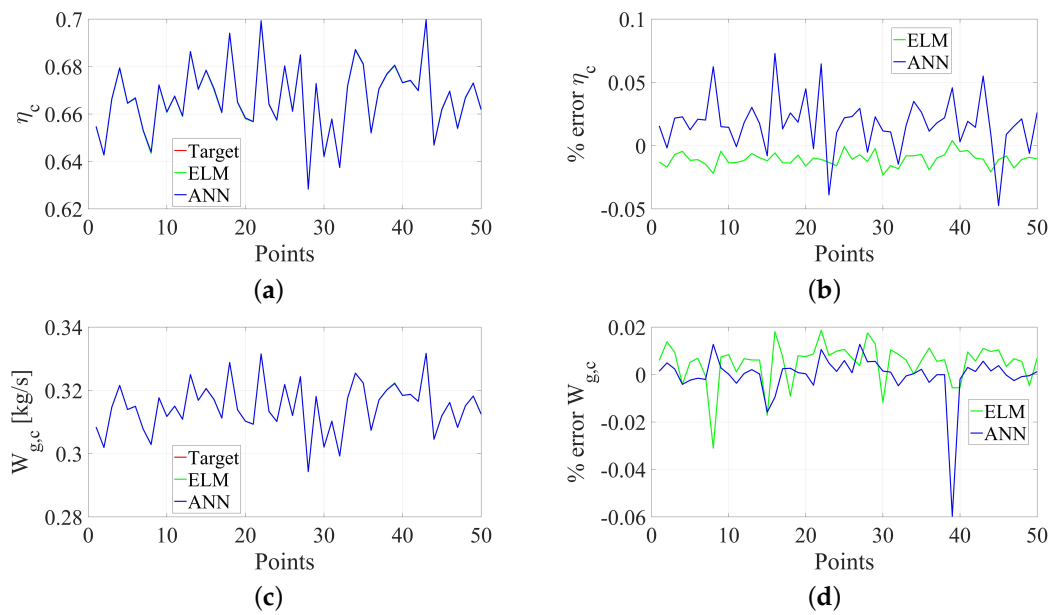


Figure 8. Compressor degradation in Flight regime 1 with Input vector 1: comparison between the target and prediction of the component performance parameters

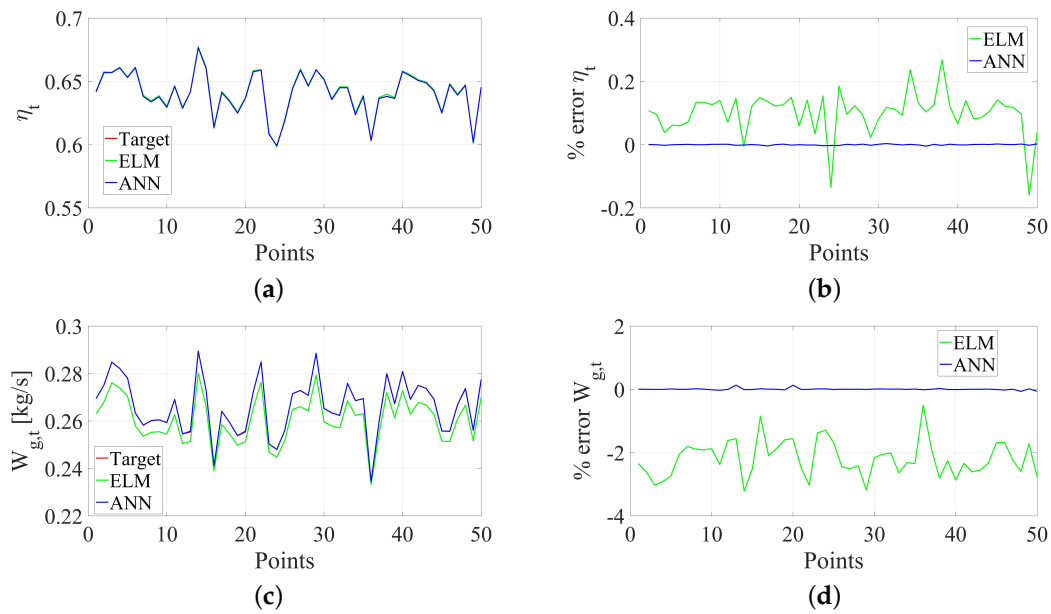


Figure 9. Turbine degradation in Flight regime 1 with Input vector 1: comparison between the target and prediction of the component performance parameters

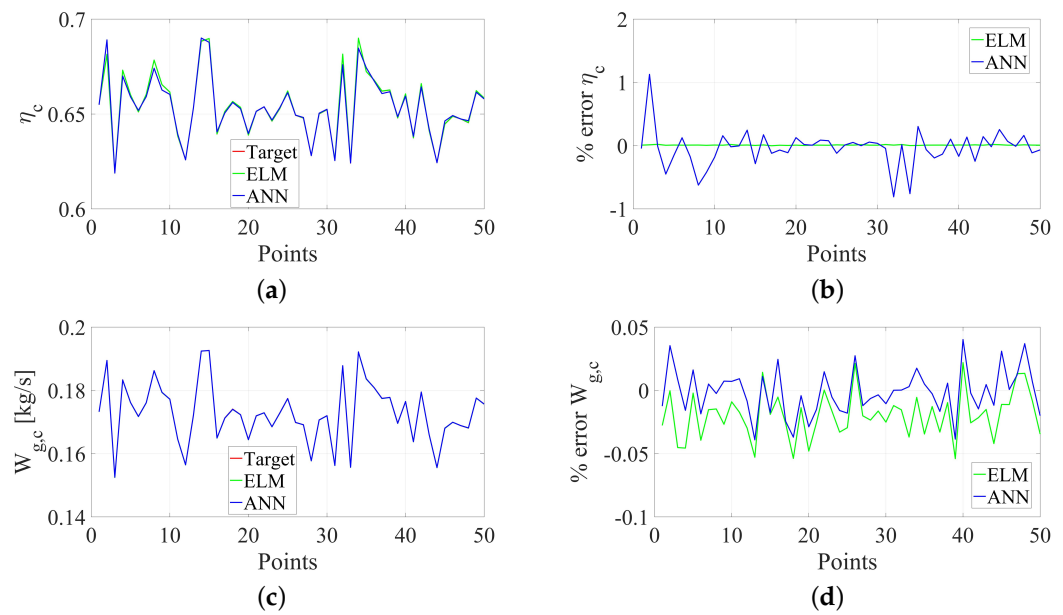


Figure 10. Compressor degradation in Flight regime 2 with Input vector 1: comparison between the target and prediction of the component performance parameters

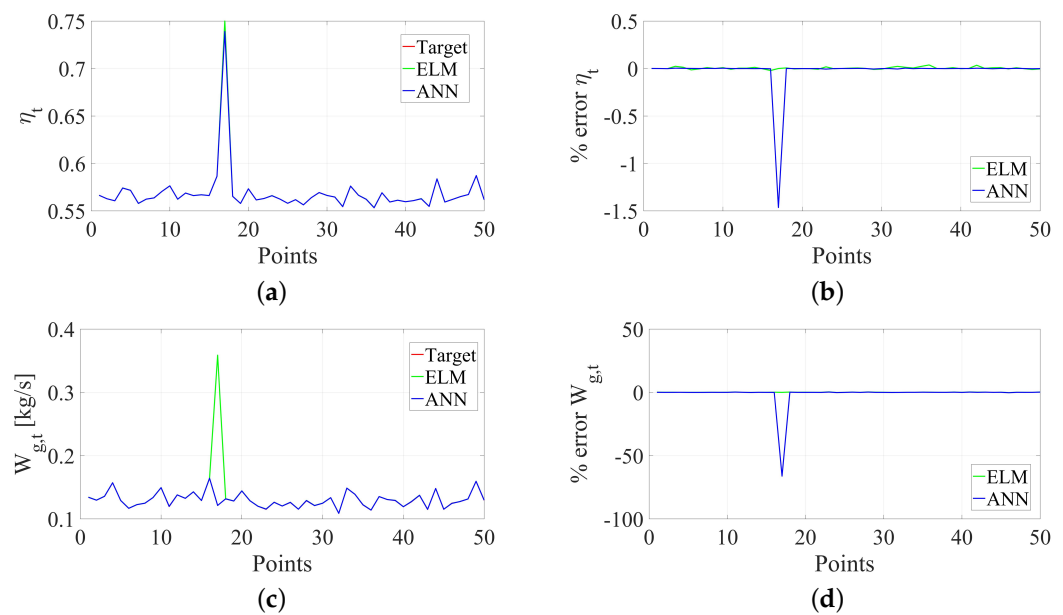


Figure 11. Turbine degradation in Flight regime 2 with Input vector 1: comparison between the target and prediction of the component performance parameters

Finally, the last scenario analyzed with extensive input vector (Input vector 2) was the dataset with various Mach and altitude (flight regime 3). Figure 12 and 13 show the results of ANN and ELM predictions. A lower accuracy is present, especially for the prediction of $W_{g,c}$.

In this case, both in η_c and $W_{g,c}$ prediction, better results are shown by the ANN, which percentage errors approach 0, except for an isolated step. In particular, the prediction of $W_{g,c}$, the error obtained from ELM application are relatively higher than at constant Mach, even if just below 4%. In Figure 13 the higher accuracy of ELM is evident, both in η_t and $W_{g,t}$ prediction. Otherwise, except for a peak in the first step (about 0.4%), the results obtained from the application of ANN are still acceptable, also in this case.

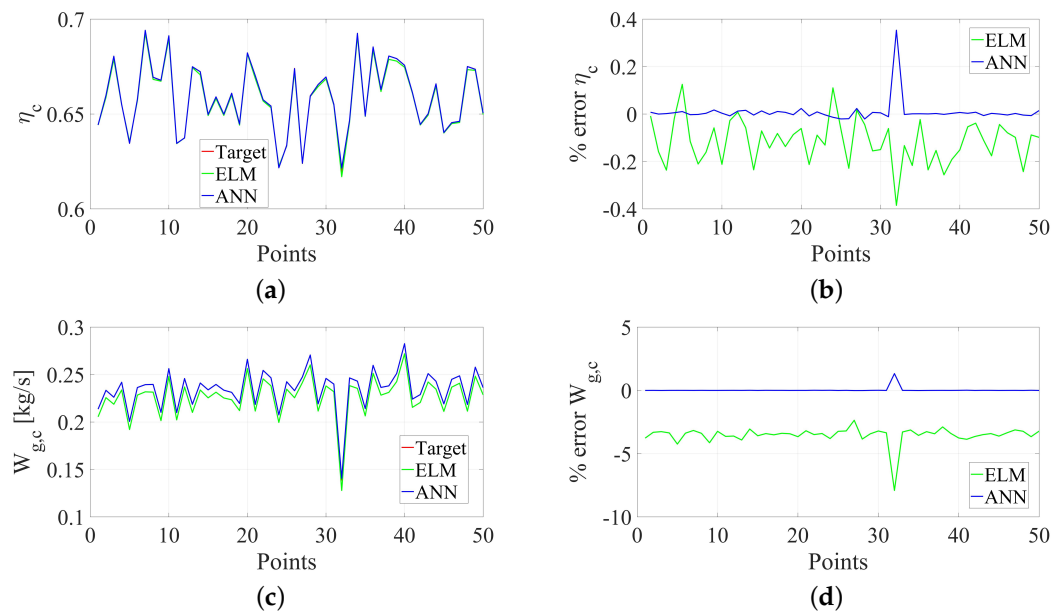


Figure 12. Compressor degradation in Flight regime 3 with Input vector 2: comparison between the target and prediction of the component performance parameters

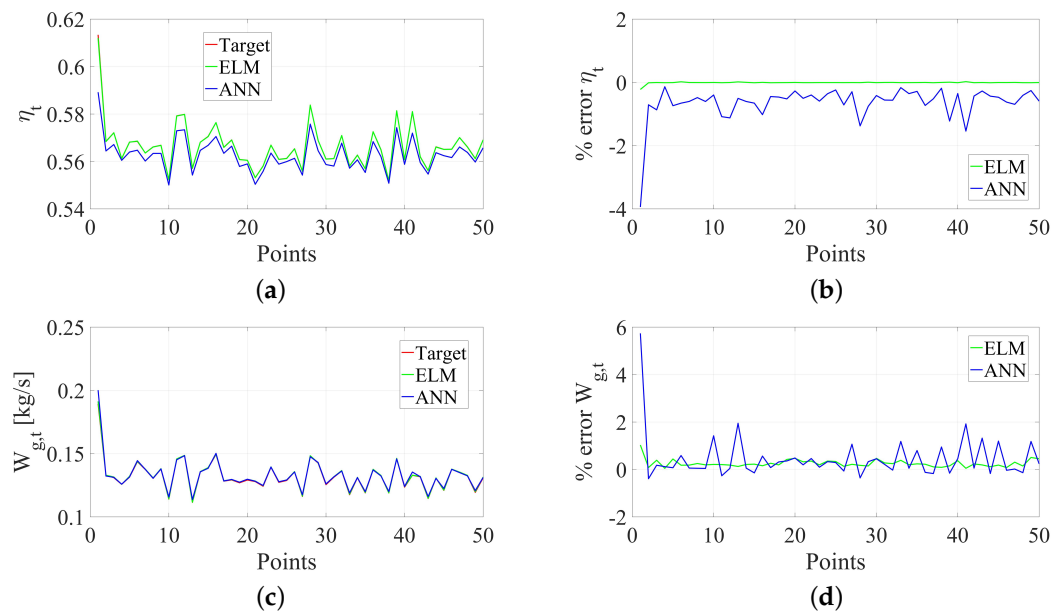


Figure 13. Turbine degradation in Flight regime 3 with Input vector 2: comparison between the target and prediction of the component performance parameters

3.3. ELM prediction with a reduced number of virtual sensors (Input vectors 3 and 4)

It is well known that feature selection i.e. choosing input parameters has a significant impact on the predictions accuracy of neural networks [40,41]. In this section, the prediction results obtained by ELM with a reduced dataset are reported. The chosen input variables correspond to the sensors that are really installed on the micro turbojet, i.e. exhaust gas temperature (EGT) and fuel flow rate. Fortunately, the performance deterioration of the aircraft engine mainly affects these two parameters, so they are well related to the efficiencies and flow capacities of compressor and turbine.

Figures 14 and 15 show the error in the prediction of the components performances under different flight regimes. Reducing the input variables decreases the accuracy of ELM with respect to the case with many sensors, especially for the turbine. In particular, the

prediction is slightly worse for the flight regime 3 with some peaks of error around 5% and 30% in the case of efficiency and mass flow respectively. These peaks are due to the imbalanced distribution of samples in training set, given by the Monte Carlo, which can hinder the performance of ELM severely.

In ideal training sets, samples of different range of the target generally obey uniform distribution, but in Monte Carlo as well as in real flight data, the number of samples of some classes of target parameters may be several times higher than that of other classes. Hence, the ELM cannot learn from minority classes effectively. Consequently, the trained network often recognize majority class samples more accurately than minorities. This is more critical than reducing the number of input variables.

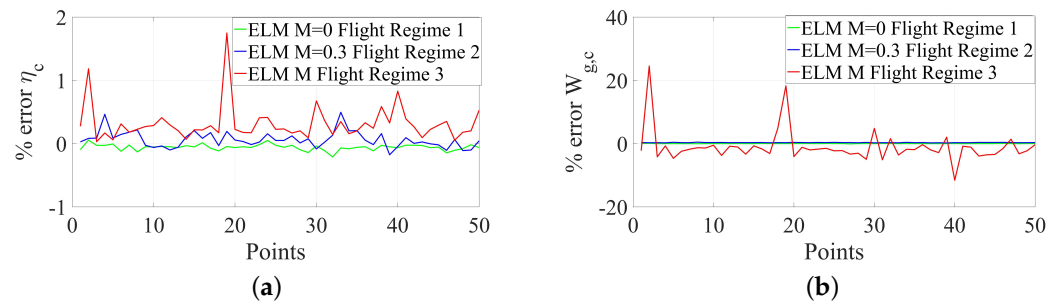


Figure 14. ELM error of compressor degradation prediction with input vector 3 or 4.

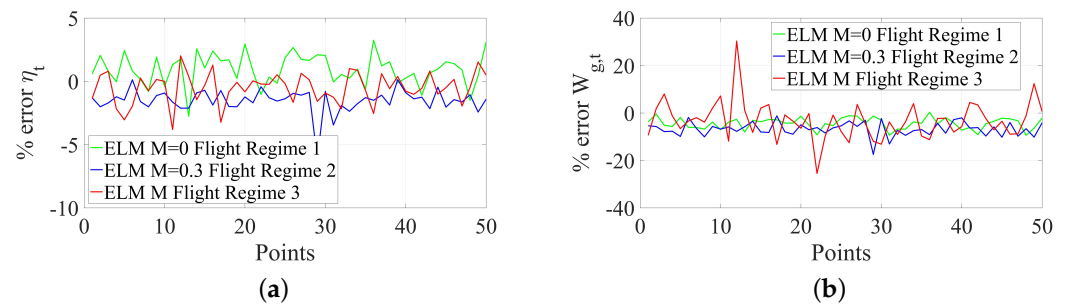


Figure 15. ELM error of turbine degradation prediction with input vector 3 or 4.

Finally, ELM was used for the prediction of compressor performance in healthy conditions (without degradation), with input vector 4 and the assumed variation of Mach number and altitude. Figure 16 shows that the accuracy in this case is very high. Hence, using the prediction of healthy and degraded performance at the same operating flight regime, it is possible to classify the health status of the components by comparing the values of the performance parameters in healthy and degraded conditions. In our earlier publications [6,40], we introduced a component degradation class ranging from 1 to 7, which combines reduced efficiency and mass flow in a single number, and is convenient for taking informed go/no-go decisions.

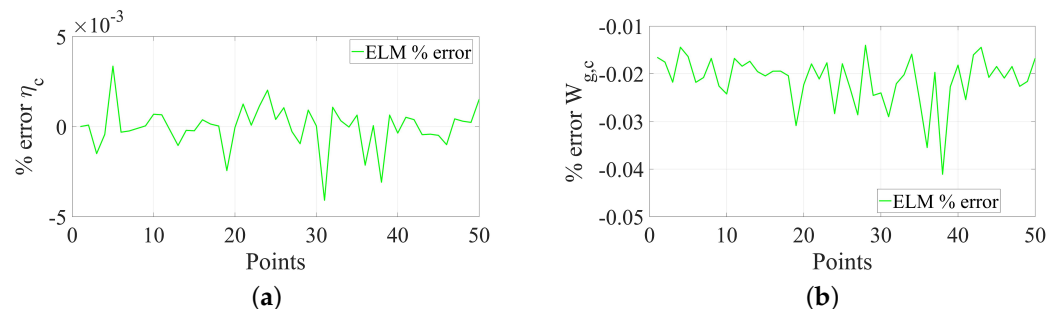


Figure 16. ELM error for compressor performance prediction under healthy conditions.

3.4. Overall accuracy metrics

The goodness of fit was evaluated in several ways to compare the results obtained from the sensitivity analysis and as a measure of the network's prediction quality. In particular, the following metrics were used:

- Normalized root mean squared error (NRMSE)
- Coefficient of determination (CoD)
- Maximum relative absolute error (MaxRAE)

The NMSE is used to measure the average squared difference between the estimated values and the actual:

$$NMSE = \frac{1}{s} \sum_{i=1}^s E_i^2 \quad (5)$$

where

$$E_i = \frac{\hat{y}_i - y_i}{std(y)} \quad (6)$$

where \hat{y}_i represents the prediction of a parameter, y_i – its actual value, s is the number of observations and $std(y)$ – the standard deviation of the actual values. Normalizing the mean squared error facilitates the comparison between datasets or models with different scales. Normalization was done by the variance of \hat{y}_i .

Coefficient of Determination (CoD) is a measure of the goodness of fit of a model and can reach one for the perfect fit:

$$CoD = 1 - \frac{\sum_{i=1}^s (y_i - \hat{y}_i)^2}{\sum_{i=1}^s (y_i - \bar{y})^2} \quad (7)$$

Relative Absolute Error (RAE) can range from zero to one. The maximum RAE should be close to zero for a good model:

$$MaxRAE = \max_{i=1}^s \frac{|\hat{y}_i - y_i|}{y_i} \quad (8)$$

Table 5 shows that the implemented prediction methods give good results in all of the degradation scenarios, as confirmed by high CoD values. At each set of conditions, the prediction of the degradation level in the compressor outperforms the performance of the turbine degradation prediction in terms of regression, however, in most cases the MaxRAE is higher in the compressor case than in the turbine degradation.

Table 5 confirms that the use of an extensive input variables leads to high prediction accuracy with slightly worse performance in the case of turbine degradation in off design conditions (flight regime 3). However, the use of few sensors in this flight regime reduces significantly prediction performance, with maxARE reaching 0.34 (Table 6).

Finally, Table 7 reports the comparison of the training time for ANN and ELM for the three flight regimes and Input Vectors 1 and 2, which is remarkably lower for ELM.

Table 5. Metrics for Input Vectors 1 and 2 ELM and ANN

		NMSE ELM	NMSE ANN	CoD ANN	CoD ELM	MaxARE ANN	MaxARE ELM
Degradation of Compressor – Flight Regime 1							
η_c	Train	2.5e-05	0.012	0.98	0.99	0.0533	2.73e-04
$W_{g,c}$	Train	1.6e-05	3.5e-06	0.99	0.99	2.80e-04	2.83e-04
η_c	Test	2.8e-05	1.5e-04	0.99	0.99	4.73e-04	2.32e-04
$W_{g,c}$	Test	1.6e-05	1.6e-05	0.99	0.99	5.97e-04	3.10e-04
Degradation of Compressor – Flight Regime 2							
η_c	Train	1.4e-05	0.0181	0.98	0.99	0.0179	3.81e-04
$W_{g,c}$	Train	1.7e-05	1.6e-05	0.99	0.99	7.2e-04	8.32e-04
η_c	Test	1.5e-05	0.012	0.98	0.99	0.0082	1.6e-05
$W_{g,c}$	Test	2.2e-04	1.1e-05	0.99	0.99	3.7e-04	5.4e-04
Degradation of Compressor – Flight Regime 3							
η_c	Train	0.002	2.1e-05	0.99	0.99	0.0018	0.003
$W_{g,c}$	Train	0.130	0.0477	0.96	0.90	2.9e-04	0.080
η_c	Test	0.003	2.9e-04	0.99	0.98	2.1e-04	0.004
$W_{g,c}$	Test	0.141	1.4e-04	0.99	0.98	1.4e-04	0.086
Degradation of Turbine – Flight Regime 1							
η_t	Train	0.002	8.5e-07	0.99	0.99	3.1e-04	0.005
$W_{g,t}$	Train	0.188	3.1e-05	0.99	0.75	0.0013	0.044
η_t	Test	0.002	4.4e-07	0.99	0.99	4.8e-05	0.002
$W_{g,t}$	Test	0.273	4.6e-05	0.99	0.71	6.3e-04	0.033
Degradation of Turbine – Flight Regime 2							
η_t	Train	1.8e-04	0.0031	0.99	0.99	0.0159	0.0031
$W_{g,t}$	Train	2.3e-04	1.3e-04	0.99	0.99	0.0025	0.0016
η_t	Test	5.9e-06	0.0033	0.99	0.99	0.014	2.1e-04
$W_{g,t}$	Test	3.0e-05	0.95	0.97	0.99	1.957	0.0018
Degradation of turbine – Flight Regime 3							
η_t	Train	4.8e-04	0.188	0.85	0.99	0.1037	3.35e-04
$W_{g,t}$	Train	4.7e-04	0.0257	0.97	0.98	0.1535	3.32e-04
η_t	Test	3.9e-04	0.24	0.85	0.99	0.041	0.0022
$W_{g,t}$	Test	0.0013	0.019	0.98	0.98	0.0039	4.8e-04

Table 6. ELM - metrics for reduced Input Vectors 3 and 4

		Compressor			Turbine		
		NMSE	CoD	MaxARE	NMSE	CoD	MaxARE
Flight Regime 1							
η	Train	0.0012	0.99	0.0065	0.3663	0.91	0.038
W	Train	1.5e-04	0.99	8.4e-04	0.7445	0.85	0.135
η	Test	0.0010	0.99	0.0021	0.300	0.90	0.0284
W	Test	1.7e-04	0.99	7.61e-04	0.8404	0.84	0.1037
Flight Regime 2							
η	Train	0.0023	0.99	0.0091	0.65	0.88	0.0388
W	Train	0.0027	0.99	0.010	0.44	0.89	0.1782
η	Test	0.0036	0.99	0.0018	0.97	0.86	0.0652
W	Test	0.0039	0.99	0.0023	0.69	0.87	0.2114
Flight Regime 3							
η	Train	0.0076	0.97	0.0054	0.10	0.81	0.05
W	Train	0.10	0.80	0.0876	0.23	0.71	0.307
η	Test	0.0247	0.99	3.6e-04	0.10	0.80	0.039
W	Test	0.1234	0.85	0.1307	0.18	0.74	0.34

Table 7. Mean training time (in arbitrary CPU units)

Flight regime	ANN	ELM
1	3.9	1.65
2	4.7	1.20
3	2.79	0.43

4. Conclusions

In this paper, ELM was used to predict the efficiency and mass flow of the compressor and turbine, which are the main components of a micro turbojet. A digital twin engine of the real engine, already validated with experimental data from a test bench and real flights, gathered in the absence of degradation, was used. The validated model was subsequently extended to predict degraded engine performance. It was used to generate a dataset containing engine operating parameters for different degradation severity conditions by means of a Monte-Carlo technique.

It was found that component degradation in the microturbine has a higher impact in a high-altitude flight than at sea level. A significant rise in the TSFC was observed when the components' efficiency decreased, especially at $M=0.3$.

The generated dataset was used to train the developed neural network with the ELM approach. Different lengths of the input vector were analyzed: an extensive one with a dozen of sensors and a reduced one with input variables corresponding to the real sensors installed on the engine. Furthermore, three different flight regimes were tested.

The analysis underlined that in presence of many input variables, ELM has good prediction accuracy, comparable with ANN, but with a shorter CPU time. However, the reduced number of sensors gives satisfactory predictions for the healthy conditions but worst accuracy for the degraded cases. Mean errors are generally acceptable but they reached 20% in few conditions in the case of off-design flight conditions (with variable Mach and altitude). The prediction performance was still satisfactory in cruise with the fixed Mach number and altitude and at sea level.

Future work will involve testing the with the real flight data collected from several operated engines. Besides formal arrangements, this may require preprocessing the data and implementing a more advanced version of ELM with regularization.

Author Contributions: Conceptualization, M.G.D.G. and N.M; methodology, N.M, M.G.D.G., A.M. and R.P; software, N.M. and A.M.; validation, N.M, R.P. and M.G.D.G.; investigation, N.M., M.G.D.G. and A.M.; data curation, N.M; writing—original draft preparation, N.M, M.G.D.G., A.M. and R.P; writing—review and editing, R.P. and M.G.D.G.; visualization, N.M, A.M. and M.G.D.G.; supervision, M.G.D.G., A.F. and R.P.; project administration, A.F. All authors have read and agreed to the published version of the manuscript.

Funding: This research was funded by the Italian Ministry of University and Research, project PON “SMEA”, code PON03PE_00067_5.



Institutional Review Board Statement: Not applicable.

Informed Consent Statement: Not applicable.

Data Availability Statement: Data presented in this study are available on request from The University of Salento.

Conflicts of Interest: The authors declare no conflict of interest.

References

1. Dvirnyk, Y.; Pavlenko, D.; Przysowa, R. Determination of Serviceability Limits of a Turboshift Engine by the Criterion of Blade Natural Frequency and Stall Margin. *Aerospace* **2019**, *6*, 132. <https://doi.org/10.3390/aerospace6120132>.
2. Przybyła, B.S.; Przysowa, R.; Zapałowicz, Z. Implementation of a new inlet protection system into HEMS fleet. *Aircraft Engineering and Aerospace Technology* **2020**, *92*, 67–79. <https://doi.org/10.1108/AEAT-11-2018-0289>.
3. Walsh, P.P.; Fletcher, P. *Gas Turbine Performance. Second Edition*; Blackwell Science Ltd: Oxford, UK, 2004.
4. Fentaye.; Baheta.; Gilani.; Kyprianidis. A Review on Gas Turbine Gas-Path Diagnostics: State-of-the-art Methods, Challenges and Opportunities. *Aerospace* **2019**, *6*, 83. <https://doi.org/10.3390/aerospace6070083>.
5. Sun, X.; Jafari, S.; Miran Fashandi, S.A.; Nikolaidis, T. Compressor Degradation Management Strategies for Gas Turbine Aero-Engine Controller Design. *Energies* **2021**, *14*, 5711. <https://doi.org/10.3390/en14185711>.
6. De Giorgi, M.G.; Campilongo, S.; Ficarella, A. A Diagnostics Tool for Aero-Engines Health Monitoring Using Machine Learning Technique. *Energy Procedia* **2018**, *148*, 860–867. <https://doi.org/10.1016/j.egypro.2018.08.109>.
7. De Giorgi, M.G.; Campilongo, S.; Ficarella, A. Development of a Real Time Intelligent Health Monitoring Platform for Aero-Engine. *MATEC Web of Conferences* **2018**, *233*, 00007. <https://doi.org/10.1051/mateconf/201823300007>.
8. Ellis, M.; Bojdo, N.; Filippone, A.; Clarkson, R. Monte carlo predictions of aero-engine performance degradation due to particle ingestion. *Aerospace* **2021**, *8*, 1–24. <https://doi.org/10.3390/aerospace8060146>.
9. Gaonkar, D.N.; Patel, R.N. Modeling and Simulation of Microturbine Based Distributed Generation System. *2006 IEEE Power India Conference* **2005**, *2005*, 256–260. <https://doi.org/10.1109/POWERI.2006.1632521>.
10. Badami, M.; Giovanni Ferrero, M.; Portoraro, A. Dynamic Parsimonious Model and Experimental Validation of a Gas Microturbine at Part-Load Conditions. *Applied Thermal Engineering* **2015**, *75*, 14–23. <https://doi.org/10.1016/j.applthermaleng.2014.10.047>.
11. Alulema, V.; Valencia, E.; Cando, E.; Hidalgo, V.; Rodriguez, D. Propulsion Sizing Correlations for Electrical and Fuel Powered Unmanned Aerial Vehicles. *Aerospace* **2021**, *8*. <https://doi.org/10.3390/aerospace8070171>.
12. Adamski, M. Analysis of Propulsion Systems of Unmanned Aerial Vehicles. *Journal of Marine Engineering and Technology* **2018**, *16*, 291–297. <https://doi.org/10.1080/20464177.2017.1383337>.
13. Minijets. The website for fans of light jet aircraft. <https://minijets.org>, accessed on 22.07.2022.
14. Pavlenko, D.; Dvirnyk, Y.; Przysowa, R. Advanced Materials and Technologies for Compressor Blades of Small Turbofan Engines. *Aerospace* **2021**, *8*, 1–16. <https://doi.org/10.3390/aerospace8010001>.
15. Oppong, F.; Spuy, S.J.V.D.; Diaby, A.L. An Overview on the Performance Investigation and Improvement of Micro Gas Turbine Engine. *R&D Journal of the South African Institution of Mechanical Engineering* **2015**, pp. 35–41. <https://doi.org/10.13140/RG.2.2.10055.09123>.
16. Capata, R.; Saracchini, M. Experimental Campaign Tests on Ultra Micro Gas Turbines, Fuel Supply Comparison and Optimization. *Energies* **2018**, *11*. <https://doi.org/10.3390/en11040799>.
17. Rahman, M.; Zaccaria, V.; Zhao, X.; Kyprianidis, K. Diagnostics-Oriented Modelling of Micro Gas Turbines for Fleet Monitoring and Maintenance Optimization. *Processes* **2018**, *6*, 216. <https://doi.org/10.3390/pr6110216>.

18. Khustochka, O.; Chernysh, S.; Yepifanov, S.; Ugryumov, M.; Przysowa, R. Estimation of Performance Parameters of Turbine Engine Components Using Experimental Data in Parametric Uncertainty Conditions. *Aerospace* **2020**, *7*(1), 1–17. <https://doi.org/10.3390/aerospace7010006>.
19. Hanachi, H.; Mechefske, C.; Liu, J.; Banerjee, A.; Chen, Y. Performance-based gas turbine health monitoring, diagnostics, and prognostics: A survey. *IEEE Transactions on Reliability* **2018**, *67*, 1340–1363. <https://doi.org/10.1109/TR.2018.2822702>.
20. de Castro-Cros, M.; Velasco, M.; Angulo, C. Machine-Learning-Based Condition Assessment of Gas Turbines—a Review. *Energies* **2021**, *14*. <https://doi.org/10.3390/en14248468>.
21. Akpudo, U.E.; Hur, J.W. Investigating the Efficiencies of Fusion Algorithms for Accurate Equipment Monitoring and Prognostics. *Energies* **2022**, *15*, 2204. <https://doi.org/10.3390/en15062204>.
22. Huang, G.B.; Zhu, Q.Y.; Siew, C.K. Extreme learning machine: Theory and applications. *Neurocomputing* **2006**, *70*, 489–501. <https://doi.org/10.1016/j.neucom.2005.12.126>.
23. Albadr, M.A.A.; Tiun, S. Extreme Learning Machine: A Review. *International Journal of Applied Engineering Research* **2017**, *12*, 4610–4623.
24. Zhao, Y.P.; Huang, G.; Hu, Q.K.; Tan, J.F.; Wang, J.J.; Yang, Z. Soft Extreme Learning Machine for Fault Detection of Aircraft Engine. *Aerospace Science and Technology* **2019**, *91*, 70–81. <https://doi.org/10.1016/j.ast.2019.05.021>.
25. Lu, F.; Jiang, C.; Huang, J.; Wang, Y.; You, C. A Novel Data Hierarchical Fusion Method for Gas Turbine Engine Performance Fault Diagnosis. *Energies* **2016**, *9*, 828. <https://doi.org/10.3390/en9100828>.
26. Jiang, W.; Xu, Y.; Shan, Y.; Liu, H. Degradation Tendency Measurement of Aircraft Engines Based on FEEMD Permutation Entropy and Regularized Extreme Learning Machine Using Multi-Sensor Data. *Energies* **2018**, *11*, 3301. <https://doi.org/10.3390/en11123301>.
27. Pérez-Ruiz, J.L.; Tang, Y.; Loboda, I. Aircraft Engine Gas-Path Monitoring and Diagnostics Framework Based on a Hybrid Fault Recognition Approach. *Aerospace* **2021**, *8*, 232. <https://doi.org/10.3390/aerospace8080232>.
28. Liu, X.; Liu, L.; Wang, L.; Guo, Q.; Peng, X. Performance Sensing Data Prediction for an Aircraft Auxiliary Power Unit Using the Optimized Extreme Learning Machine. *Sensors* **2019**, *19*, 3935. <https://doi.org/10.3390/s19183935>.
29. Bai, M.; Liu, J.; Ma, Y.; Zhao, X.; Long, Z.; Yu, D. Long Short-Term Memory Network-Based Normal Pattern Group for Fault Detection of Three-Shaft Marine Gas Turbine. *Energies* **2020**, *14*, 13. <https://doi.org/10.3390/en14010013>.
30. Berghout, T.; Mouss, L.H.; Kadri, O.; Saïdi, L.; Benbouzid, M. Aircraft Engines Remaining Useful Life Prediction with an Improved Online Sequential Extreme Learning Machine. *Applied Sciences* **2020**, *10*, 1062. <https://doi.org/10.3390/app10031062>.
31. Chen, H.; Li, Q.; Pang, S.; Zhou, W. A State Space Modeling Method for Aero-Engine Based on AFOS-ELM. *Energies* **2022**, *15*, 3903. <https://doi.org/10.3390/en15113903>.
32. Gu, Z.; Pang, S.; Zhou, W.; Li, Y.; Li, Q. An Online Data-Driven LPV Modeling Method for Turbo-Shaft Engines. *Energies* **2022**, *15*, 1255. <https://doi.org/10.3390/en15041255>.
33. Erario, M.L.; De Giorgi, M.G.; Przysowa, R. Model-Based Dynamic Performance Simulation of a Microturbine Using Flight Test Data. *Aerospace* **2022**, *9*, 60. <https://doi.org/10.3390/aerospace9020060>.
34. Visser, W.P.J.; Broomhead, M.J. GSP, a Generic Object-Oriented Gas Turbine Simulation Environment. In Proceedings of the Volume 1: Aircraft Engine; Marine; Turbomachinery; Microturbines and Small Turbomachinery. American Society of Mechanical Engineers, 2000. <https://doi.org/10.1115/2000-GT-0002>.
35. *GSP 11 User Manual*; NLR - Royal Netherlands Aerospace Centre: Amsterdam, The Netherlands, 2021.
36. *JetCat RX Turbines with V10 ECU*; Ingenieur-Büro CAT, M. Zipperer GmbH: Staufen, Germany, 2010; pp. 1–54.
37. Hajduk, J.; Rykaczewski, D. Possibilities of Developing Aerial Target System JET-2 (Możliwości Rozwoju Zestawu Odrzutowych Celów Powietrznych Zocp-Jet2). In *Mechanika w Lotnictwie ML-XVIII Tom 2 (Mechanics in Aviation ML-XVIII Volume 2)*; Krzysztof Sibilski, Ed.; PTMTS: Warszawa, Poland, 2018; pp. 139–154.
38. De Giorgi, M.G.; Quarta, M. Hybrid MultiGene Genetic Programming - Artificial Neural Networks Approach for Dynamic Performance Prediction of an Aeroengine. *Aerospace Science and Technology* **2020**, *103*, 105902. <https://doi.org/10.1016/j.ast.2020.105902>.
39. De Giorgi, M.G.; Straffella, L.; Ficarella, A. Neural nonlinear autoregressive model with exogenous input (Narx) for turboshaft aeroengine fuel control unit model. *Aerospace* **2021**, *8*. <https://doi.org/10.3390/aerospace8080206>.
40. De Giorgi, M.G.; Straffella, L.; Menga, N.; Ficarella, A. Intelligent Combined Neural Network and Kernel Principal Component Analysis Tool for Engine Health Monitoring Purposes. *Aerospace* **2022**, *9*. <https://doi.org/10.3390/aerospace9030118>.
41. Khumprom, P.; Grewell, D.; Yodo, N. Deep Neural Network Feature Selection Approaches for Data-Driven Prognostic Model of Aircraft Engines. *Aerospace* **2020**. <https://doi.org/10.3390/aerospace7090132>.